Published in final edited form as:
Biomaterials. 2011 September ; 32(26): 6119–6130. doi:10.1016/j.biomaterials.2011.05.015.

Creation of bony microenvironment with CaP and cell-derived ECM to enhance human bone-marrow MSC behavior and delivery of BMP-2

Yunqing Kang[1], **Sungwoo Kim**[1], **Ali Khademhosseini**[2], and **Yunzhi Yang**[1,*]

[1] Department of Restorative Dentistry and Biomaterials, The University of Texas Health Science Center at Houston, 6516 M.D. Anderson Blvd., Houston, Texas 77030

[2] Center for Biomedical Engineering, Department of Medicine, Brigham and Women's Hospital, Harvard Medical School, Cambridge, MA, 02139; Harvard-MIT Division of Health Sciences and Technology, Massachusetts Institute of Technology, Cambridge, MA, 02139; Wyss Institute for Biologically Inspired Engineering, Harvard University, Boston, MA 02115, USA

Abstract

Extracellular matrix (ECM) comprises a rich meshwork of proteins and proteoglycans, which not only contains biological cues for cell behavior, but is also a reservoir for binding growth factors and controlling their release. Here we aimed to create a suitable bony microenvironment with cell-derived ECM and biodegradable β-tricalcium phosphate (β-TCP). More specifically, we investigated whether the ECM produced by bone marrow-derived mesenchymal stem cells (hBMSC) on a β-TCP scaffold can bind bone morphogenetic protein-2 (BMP-2) and control its release in a sustained manner, and further examined the effect of ECM and the BMP-2 released from ECM on cell behaviors. The ECM was obtained through culturing the hBMSC on a β-TCP porous scaffold and performing decellularization and sterilization. SEM, XPS, FTIR, and immunofluorescent staining results indicated the presence of ECM on the β-TCP and the amount of ECM increased with the incubation time. BMP-2 was loaded onto the β-TCP with and without ECM by immersing the scaffolds in the BMP-2 solution. The loading and release kinetics of the BMP-2 on the β-TCP/ECM were significantly slower than those on the β-TCP. The β-TCP/ECM exhibited a sustained release profile of the BMP-2, which was also affected by the amount of ECM. This is probably because the β-TCP/ECM has different binding mechanisms with BMP-2. The β-TCP/ECM promoted cell proliferation. Furthermore, the BMP-2-loaded β-TCP/ECM stimulated reorganization of the actin cytoskeleton, increased expression of alkaline phosphatase and calcium deposition by the cells compared to those without BMP-2 loading and the β-TCP with BMP-2 loading.

Keywords

ECM (Extracellular matrix); BMP-2 (Bone morphogenetic protein-2); Beta-tricalcium phosphate (β-TCP); Bone tissue engineering; Scaffold

*Corresponding author: Yunzhi Yang, Ph.D. Assistant Professor Department of Restorative Dentistry and Biomaterials University of Texas Health Science Center at Houston 6516 M.D. Anderson Blvd., D 4.133, Houston, TX 77030, Tel: 713 - 500 4083, Fax: 713 - 500 4372, yunzhi.yang@uth.tmc.edu.

1. Introduction

Extracellular matrix (ECM) is a rich source of bioactive molecules and is mainly composed of collagens, proteoglycans, glycoproteins, and smaller amounts of other proteins [1–3]. In bone matrix, the ECM is composed of not only collagenous and non-collagenous proteins, but also an inorganic mineralized phase [4, 5]. Early work on ECM has indicated that these ECM proteins are crucial in mediating cell adhesion, cell migration, proliferation, and differentiation through cell-matrix interactions [6–8]. ECM secreted by cells may also provide many active binding sites which can bind the domain of a target growth factor receptor [9]. For example, heparan sulfate proteoglycans in ECM have specific binding with growth factors, which might result in the entrapment of growth factors into ECM [10–12].

Since the ECM plays an important role in determining how cells behave, creation of a bony environment of mimicking natural ECM may greatly improve its physiological function [13]. Some studies have reported that natural ECM extracted from animal tissues can be used directly as scaffolds for tissue engineering [14–16]. But this type of ECM scaffold is limited by the dimensions and form of the original tissue and the potential pathogen risk. Besides animal tissues, ECM also can be extracted from cultured cells, which has also been used as a biological scaffold for tissue engineering. But cell-derived ECM scaffolds lack form and structural support [17]. Therefore, most studies have been directed towards mimicking the ECM environment by incorporating ECM proteins on supportive synthetic biomaterials such as ceramics, synthetic polymers, denatured collagen, and hydrogels [18–21]. This strategy generally involves dipping a scaffold in one or multiple ECM-associated protein solutions or immobilizing silane grafted proteins or short peptide sequences derived from ECM proteins on an etched surface of a scaffold [22, 23]. The use of single or multiple proteins only provide fragmental components with specific functional receptors for cell adherence or growth [24, 25], while the native ECM is multi-functional and can influence multiple biochemical and mechanical processes simultaneously [8]. As such, modifying a synthetic scaffold with cell-derived ECM would have great potential in recapitulating the natural bony ECM microenvironment. Studies have shown that rat marrow stromal cells formed bone-matrix *in vitro* when cultured on titanium fiber mesh in the presence of osteogenic supplements, and the resulting ECM can be extracted after decellularization [7, 26, 27]. The synthetic scaffolds containing bone-like ECM secreted by the cultured cells significantly enhanced the mineralized matrix deposition of marrow stromal cells compared to those on titanium or polymeric scaffolds in the absence of the ECM [26–28].

In addition, bone repair and regeneration is a complex cascade of biological events, which involves not only ECM and bone-forming cells, but also osteogenic growth factors [29]. Many reports have shown that bone regeneration can be enhanced by sustained release of osteogenic growth factors, such as bone morphogenetic protein-2 (BMP-2) [30, 31]. BMP-2 is a widely-used, potent osteogenic growth factor and has been shown to induce osteogenic differentiation of multipotent mesenchymal cells [32, 33] and induce bone formation in both animals and humans [34, 35]. BMP-2 has been approved by FDA for clinical use in several indications in the U.S. since 2002 [36, 37]. However, a major challenge is still finding an optimal carrier for BMP-2 at the site of injury. Even though diverse growth factor delivery systems have been intensively investigated in orthopedics [38, 39], there are few reports on the use of cell-derived ECM deposited on an engineered scaffold as an effective delivery system for growth factors in a sustainable manner.

In this study, we hypothesized that a cell-derived, natural ECM deposited on a calcium phosphate (CaP) mineral substrate could present a greater potential for creation of a suitable bony environment for bone regeneration. More specifically, we investigated whether the

ECM produced by human bone marrow-derived mesenchymal stem cells (hBMSC) on a biodegradable β-tricalcium phosphate (β-TCP) scaffold can bind BMP-2 and control its release in a sustained manner and, additionally, to examine the effect of ECM and the BMP-2 released from the ECM on cell behavior. We first cultured the hBMSC on a 3D porous β-TCP scaffold, allowing the cells to secrete and deposit bone-like ECM on the surface of the scaffold. After the culture time, the scaffold constructs were decellularized, leaving the deposited ECM on the scaffold. Then BMP-2 was loaded onto the β-TCP and β-TCP/ECM scaffolds, and their effects on cell proliferation, differentiation, and mineralization were analyzed.

This β-TCP/ECM as a new growth factor delivery system potentially takes advantage of ECM binding sites to combine growth factors and to control their release as local regulators of bone cell function. As the ECM is broken down by matrix metalloproteinase, it releases the entrapped growth factors to cells [40]. In addition, the ECM and growth factors released from the ECM are interdependent, and may simultaneously present the biological cues to stimulate cellular differentiation, proliferation, migration, and adhesion [41, 42]. Therefore, we expected that the β-TCP/ECM and the BMP-2-loaded β-TCP/ECM constructs can significantly promote cell proliferation, differentiation and mineralization *in vitro*.

2. Materials and methods

2.1. Materials

β-tricalcium phosphate (β-TCP) powder with specific area of 17 m^2/g was purchased from Nanocerox Inc. (Ann Arbor, MI). Carboxymethyl cellulose (CMC) powders, paraffin granules, Rhodamine phalloidin, DAPI and anhydrous ethyl alcohol were purchased from Fisher Scientific (Pittsburgh, PA). All other chemicals were analytical grade and were used without treatment after being received.

2.2. Preparation of β-TCP scaffolds

β-TCP scaffolds with interconnected pores were prepared by a template-casting method [43]. The method includes the preparation of paraffin beads and β-TCP ceramic slurry, casting the slurry into a mold filled with paraffin beads, solidifying, and sintering. Paraffin beads were prepared by a conventional water-dispersion method [43]. The paraffin beads with particle sizes between 0.71 and 1 mm were used in this study. The β-TCP powder, CMC powder, dispersant (Darvan C) and surfactant (Surfonals) were mixed with distilled water while stirring to form the ceramic slurry. After filling the paraffin beads into the customized molds, the β-TCP slurry was cast into the molds under a vacuum. The as-cast mold with slurry was dehydrated and solidified in a series of ethyl alcohol solutions, typically 70, 90, and 95% at 40–70 °C. After removing the dehydrated green body from the mold, the green body was put into an electric furnace and heated up to 1250 °C for 3 h to sinter the β-TCP scaffolds. A schematic graph of the fabrication process is shown in Fig. 1. The pore size, porosity and compressive strength of the scaffolds were characterized as described in our previous publication [43]

2.3. Cell culture

Human bone marrow-derived mesenchymal stem cells (hBMSC) purchased from Lonza (Allendale, NJ) [44] were cultured in Dulbecco's modified Eagle's medium (DMEM) supplemented with 10% FBS, 1% L-Glutamine, 1% antibiotic-antimycotic solution. Medium was generally changed every 3 days. Passage 6–8 hBMSCs were used in this study.

2.4. Generation of β-TCP/ECM scaffolds

Cells were cultured in 75 cm^2 flasks in DMEM. The cells were trypsinized, resuspended in a known amount of medium and seeded onto the scaffold at 1×10^5 cells/scaffold. Scaffolds were incubated for 1 h with the seeding cell suspension for the initial attachment, after which DMEM medium supplemented with 10% FBS, 1% L-Glutamine, 1% antibiotic-antimycotic solution and osteogenic factors (10 nM dexamethasone, 50 μg/mL L-ascorbic acid and 10 mM β-glycerophosphate) was added. The medium was generally changed every 3 days. Cell/scaffold constructs were cultured for 7 days and 14 days in complete osteogenic medium. At the end of the culture period, constructs were rinsed in PBS and stored in sterile deionized water at −80 °C for later use.

The cellular component of the cell/scaffold constructs was removed to generate the scaffolds with deposited ECM. β-TCP/ECM was designated as β-TCP/ECM-7 for 7 days culture and β-TCP/ECM-14 for 14 days culture. Scaffolds were thawed at 37 °C for 20 min, rinsed with distilled water to remove cellular debris, and frozen in −80 °C for 20 min. Constructs underwent three repetitions of freeze/thaw −80 °C/37 °C cycles under sterile conditions to ensure complete removal of the cellular component. Samples were then allowed to freeze-dry. As a control, one group of cell-free scaffolds was soaked in the same culture medium and similarly processed.

2.5. Characterization of ECM on the scaffold

2.5.1. The immunofluorescent staining of ECM—After decellularization, β-TCP/ECM scaffolds were washed in PBS three times. The samples were blocked using a 3% BSA-PBS serum solution at room temperature for 30 min and incubated with rabbit anti-mouse primary antibodies for collagen I (dilution 1:100, Abcam) in 1% BSA-PBS overnight at 4 °C. Then, the samples were washed with PBS twice and the secondary antibody (Alexa Fluor 488, goat anti-rabbit, Invitrogen) in 1% BSA-PBS (diluted 1:250) was added for 1 hr at room temperature while protected from light, rinsed three time in PBS, and then were imaged by fluorescent microscopy (Nikon 2000).

2.5.2. Scanning electron microscopy (SEM) analysis—The cell/β-TCP scaffold and β-TCP/ECM scaffold after decellularization were fixed with 2.5% gulutalaldehyde in PBS for 1 h. After being thoroughly washed with PBS, the samples were dehydrated sequentially in 70%, 90%, 95% and 100% ethanol for 15 min each time. The fixed samples were dried completely, sputter-coated with gold, and examined under a scanning electron microscope (FEI, USA) operated at 15 kV voltages. The control scaffold was similarly treated and observed by SEM.

2.5.3. X-ray photoelectron spectroscopy (XPS) measurement—Surface element analysis of ECM on β-TCP was conducted using XPS. The XPS measurements can probe a maximum sampling depth of approximately 3–5 nm and therefore provide information about surface chemistry. The XPS measurements were carried out on a PHI Quantera XPS with a focused monochromatic Al Kα X-ray (1486.6 eV) source for excitation. X-rays at 40 W, 15 kV and 200 μm diameter were used to bombard the sample. The XPS survey scan spectra in the 1100–0 eV binding energy range were recorded in 0.5 eV steps with a pass energy of 140 eV. For each sample, high resolution element scan spectra of C1s, O1s, N1s, Ca2s, P2p were recorded in 0.1 eV steps with a pass energy of 26 eV. All binding energies were autoshift scaled to the C1s photoelectron peak at 284.7 eV. The percentages of each major element in ECM were calculated by the software program Multipak associated with the equipment.

2.5.4. Infrared spectra in attenuated total reflection (ATR-FTIR) measurement

—ATR-FTIR analysis of β-TCP/ECM was performed using the Golden Gate reflection diamond ATR systems on a Nicolet spectrometer. The ATR accessory contained a ZnSe crystal. ATR-FTIR spectra (100 scans at 4.0 cm^{-1} resolution and ratioed to the appropriate background spectra) were recorded at 25 °C. A special dry system was constructed to prevent interference of atmospheric moisture with the spectra.

2.6. BMP-2 loading on β-TCP/ECM scaffolds

To load BMP-2 (Peprotech, Rocky Hill, NJ) onto the β-TCP/ECM scaffolds, each scaffold was weighed and immersed in corresponding volume of a BMP-2 solution (1.5 μg/mL) according to the weight/volume ratio (8 mL per gram). Then, the samples were incubated at room temperature for 1, 2, 4, 8, 12, 24 hours with gentle shaking. At the designated time point, 10 μL of the solution was removed and the concentration of BMP-2 was measured by a BMP-2 ELISA kit (R&D Systems). After 24 hrs absorption, the scaffolds were taken out of the solution and washed three times in PBS. The β-TCP/ECM scaffolds loaded with BMP-2 were freeze-dried under sterile conditions and stored at −20 °C for later use. Three groups of scaffolds were loaded BMP-2 via this process, including the β-TCP/ECM-7, the β-TCP/ECM-14, and the β-TCP as a control.

2.7. In vitro release profile of BMP-2 from β-TCP/ECM scaffolds

To investigate the *in vitro* release profile of BMP-2 from the β-TCP/ECM scaffolds, the BMP-2-loaded scaffolds were put into a vial containing 1mL DMEM culture medium. The vials were incubated at 37 °C for 5 weeks. At the end of each time point, the release medium was collected and totally replaced with equal amount of fresh DMEM medium. The amount of released BMP-2 was measured using a BMP-2 ELISA kit. The release profile was calculated in terms of the cumulative release percentage of BMP-2 (%, w/w) with incubation time. Each experiment was carried out in triplicate.

2.8. Biological effects of β-TCP/ECM and BMP-2-loaded β-TCP/ECM

2.8.1. Effect on the proliferation and differentiation of hBMSC—

To assess proliferation and osteogenic differentiation of hBMSCs on the β-TCP/ECM and BMP-2-loaded β-TCP/ECM scaffolds with various ECM maturities, six groups of scaffolds were used in this experiment: (1) β-TCP/ECM-7; (2) β-TCP/ECM-14; (3) β-TCP, as a control; (4) β-TCP/ECM-7/BMP-2, in which the BMP-2 was loaded to the sterilized β-TCP/ECM-7; (5) β-TCP/ECM-14/BMP-2, in which the BMP-2 was loaded to the sterilized β-TCP/ECM-14; and (6) β-TCP/BMP-2, in which the BMP-2 was loaded to the sterilized β-TCP. hBMSCs were seeded onto the scaffolds at a seeding density of 100,000 cells in 100 μL of DMEM medium without osteogenic factors. Scaffolds were incubated for 1 h with the seeding cell suspension for the initial attachment, after which DMEM medium was added to each well of the 24-well plates and cultured for 3, 7, 10 and 14 days with medium changed every 2–3 days. Three samples per group per time point were used. At the end of each time point, samples were rinsed with PBS (without calcium and magnesium) and stored at −20°C for later analysis.

Double stranded DNA (dsDNA) that represents for cell proliferation was determined in a fluorometric assay. Samples taken from culture were rinsed with PBS. Cell lysate was prepared by lysing cells in 0.2% Triton-X-100 via three repetitions of a freeze and thaw cycles, in which samples were frozen for 20 min in −80°C then thawed for 20 min in a 37°C water bath, and finally sonicated for 1 min on ice to allow DNA into the solution. DNA was quantified using the PicoGreen assay (Invitrogen, Carlsbad, CA) according to the manufacturer's instructions. DNA concentration was measured on a plate reader (BioTek

FL800) through fluorescence at 520 nm and compared to a standard curve generated from known concentrations of DNA standards.

Alkaline phosphatase activity (ALP) as an early osteogenic differentiation marker was determined with p-nitrophenyl phosphate (p-NPP) substrate in a colorimetric assay [45]. Cell lysates were placed in a 96-well plate, and the reaction was allowed to progress for 30 min at 37 °C. After incubation, samples were placed on ice and 100 μL of 1 M sodium hydroxide was added to stop the reaction. The resultant absorbance values were measured at 405 nm in a microplate reader (BioTek FL800, USA) and compared to a standard curve generated from known concentrations of p-nitrophenol standards. ALP activity was normalized to dsDNA concentration from the same sample and expressed as units per gram of dsDNA.

2.8.2. Effect of ECM and ECM/BMP-2 on cell F-actin expression—

Microfilamentous actins (F-actin) participate in many important cellular processes, including cell mobility, cell division, cell signaling, and establishment of gap junctions and cell shape. BMP-2 was reported to rearrange F-actin in cells and regulate the function of cells [46, 47]. To observe the filamentous F-action fiber expression of cells, the scaffolds were put in the insert wells of 24-well plates. The hBMSC cells were seeded on the bottom of the wells. Culture medium was changed every 3 days. After 3 days, cells were washed twice with PBS (pH 7.4) and fixed by 4% paraformaldehyde solution (PFA) in PBS for 15 min at room temperature. After washing twice with PBS, the cells were permeabilized in 0.5% Triton-X-100 in PBS and incubated in freshly prepared Rhodamine phalloidin (stock solution diluted in 1:100, cytoskeleton Inc. USA) at room temperature for 2 hours, and after a brief PBS wash, DAPI solution (5 μg/mL) was added for counterstaining cell nuclei. Confocal images were performed on a confocal laser scanning microscope (CLSM, Olympus IX81). To assess the effect of ECM and/or BMP-2 on the F-actin synthesis, the exposure time for each fluorescent channel of CLSM on each sample was the same and random images were taken from six random fields/well at a magnification of 20×. The fluorescent intensity of F-actin per cell was calculated by the software program Slide 5 associated with the CLSM instrument.

2.8.3. Effect of β-TCP/ECM and β-TCP/ECM/BMP-2 on cell matrix mineralization—

We next investigated the ability of hBMSC to deposit calcium mineral nodules *in vitro* by Alizarin red S in the presence and absence ECM and BMP-2 on CaP scaffolds. Alizarin red S has been widely used to assess the mineralization by staining calcium deposits. As the β-TCP also contains calcium, the Alizarin red S assay could not differentiate the calcium minerals by cells from the calcium of the scaffolds. Therefore, the experiment set-up was redesigned as follows: the scaffolds were put in a multiwell insert, and the cells were seeded on the bottom wells of the 24 well plates. Culture medium was changed every 3 days. Alizarin red S staining was performed to assess calcium deposition. After 14 and 21 days of incubation, cells were washed twice with Ca and Mg-free PBS buffer and fixed with 95% ethanol for 15 min. The fixed cells were then washed twice with deionized water and stained with 1 mg/mL Alizarin red S in distilled water (pH 4.2) for 30 min at room temperature. After washing five times with deionized water, the calcium mineral nodules were examined under a microscope. To quantify the deposited calcium, the bound alizarin red S stain was extracted for 30 min while rocking. The extraction medium consisted of 10% acetic acid and methanol. The extracts were transferred to a 96-well plate and measured at 450 nm in a plate reader for the determination of mineralization by comparison with Alizarin Red S standards. Alizarin Red S binds about 2 mol of Ca^{2+}/mol of dye in solution [48].

2.9. Statistical analysis

All the groups in the experiments were performed in triplicate, and values were reported as mean values ± SD and statistically analyzed using student's *t*-test between two groups. The difference was considered to be significant if *p*-values obtained from the test were less than 0.05.

3. Results

3.1. Characterization of β-TCP scaffolds

In this study, porous β-TCP scaffolds were fabricated by a template-casting method. SEM observation in Fig.1 shows a porous structure and the interconnected windows between pores of a scaffold. These interconnected windows were formed due to the template structure, in which the paraffin beads were partially melted together during the heating process (Fig.1). In this study, the porosity and pore size of the scaffolds were 82.49 ± 0.04% and 350–500 μm, respectively, and the compressive strength of the scaffolds was 3.41 ± 0.3 MPa.

3.2. Characterization of ECM generated on β-TCP scaffolds

3.2.1. SEM morphologies and immunofluorescent staining—To obtain ECM with different maturities, cells/scaffolds were cultured for 7 days and 14 days, and then decellularized. Fig. 2 shows the changes of surface morphology of the scaffolds with different incubation time. The plain scaffold surfaces showed micrograins and micropores, and no significant differences in surface morphologies are observed on the scaffolds before (Fig.2A) and after (Fig.2B) immersion in medium without cells. The hBMSCs proliferated well on the scaffolds (Fig. 2C and 2E). After 7 days of incubation, there were many filopodia among the cells, and the scaffold surface was partially covered by the proliferating cells and their synthesized ECM (Fig.2C). After 14 days of incubation, cells spread out on the scaffold and the surface was entirely covered by cells and their deposited ECM (Fig. 2E). After decellularization and EO gas sterilization, residual aggregations and layers of the ECM can be observed on the scaffolds (Fig. 2D and 2F).

One major component of ECM, collagen type I, was evaluated by immunofluorescent staining and the results are presented in Fig.3. The fluorescent images revealed that collagen type I, an indicator of ECM, was present on the scaffold after decellularization and EO gas sterilization (Fig. 3A, B). The collagen type I produced by hBMSC was present on the inner wall and strut surfaces of the scaffolds, suggesting the cells grew on the strut surface and migrated into the inner walls of the macroporous scaffolds. Fig.3B further suggests that the ECM was still present in the porous scaffold after the gas sterilization.

3.2.2. *XPS* analysis—XPS measurements were carried out to survey the elements in the ECM deposited on the β-TCP scaffolds. Fig.4 shows that a new element peak corresponding to N1s (binding energy, 400 eV) appeared on both the β-TCP/ECM-7 and the β-TCP/ECM-14 after decellularization and extensive washing in distilled water, while it remained absent on the β-TCP. The nitrogen peak observed could be attributed to the amino groups on the scaffold surface [49]. It was also observed that the C1s peak (binding energy, 284.7 eV) on the surface of the β-TCP/ECM-7 and β-TCP/ECM-14 was greater than that of the β-TCP. Table 1 further indicates that the N atomic percentage in the β-TCP was zero, but it increased to 6.4% and 8.2% in the β-TCP/ECM-7 and the β-TCP/ECM-14, respectively. The C atomic percentage in the β-TCP/ECM-7 and the β-TCP/ECM-14 was also significantly higher than that in the β-TCP: up to 39.1% and 26.9% compared to the 6.5% in the β-TCP without the deposited ECM. Trace amounts of C atoms in the β-TCP may result from the residue of carbon-containing chemical reagents used in the sample preparation process.

Taken together, these results indicated protein biomolecules of the ECM, secreted by hBMSC, were presented on the surface of the scaffolds.

3.2.3 *FTIR* analysis—The ATR-FTIR analysis was performed to further characterize the constituents of the ECM deposited on the β-TCP. The FTIR spectra from Fig. 5 indicate that two new adsorption bands, at 1642.4 cm^{-1} and 3389.3 cm^{-1} appeared in the β-TCP/ECM-7 and the β-TCP/ECM-14 spectra that were absent in the β-TCP spectrum. These two new absorption peaks on the β-TCP/ECM spectrum are assigned to amide I and hydroxyl groups, respectively [50]. The amide group is probably a result of collagen protein in ECM. The hydroxyl group is probably a result of proteoglycans which contain many hydroxyl groups in their molecular structure [49]. The intensity of these two peaks in the β-TCP/ECM-14 spectrum was much stronger than that in the β-TCP/ECM-7 spectrum, suggesting a greater amount of ECM in the β-TCP/ECM-14 because of the longer time of incubation. These peaks were absent in the β-TCP spectrum. A wide band from 900–1200 cm^{-1} was assigned for the characteristic bands of phosphate in the β-TCP [51].

3.3. Loading kinetics and in vitro release profiles of BMP-2

Loading of BMP-2 on the β-TCP in the presence and absence of ECM was detected by an ELISA kit. The amount of the BMP-2 adsorbed on the β-TCP rapidly increased with the incubation time (Fig.6). The adsorption of the BMP-2 on the β-TCP almost reached the plateau after 4 hrs, while the loading amount of the BMP-2 gradually increased for the β-TCP/ECM-7 and the β-TCP/ECM-14, respectively, and equilibrium was not achieved until 12 hours (Fig.6). Furthermore, the loading kinetics of BMP-2 on the β-TCP/ECM-14 was significantly slower than that on the β-TCP/ECM-7 between 1 and 7 hours. Similarly, the loading kinetics of the BMP-2 on the β-TCP/ECM-7 was slower than that on the β-TCP. After 12 hours of incubation, the amount of BMP-2 loaded on the scaffolds reached the equilibrium. No significant differences in the amount of BMP-2 loaded were observed among the three groups of scaffolds after 24 hrs.

The release kinetics of the BMP-2 was investigated by immersing the β-TCP/BMP-2, the β-TCP/ECM-7/BMP-2, and the β-TCP/ECM-14/BMP-2 into cell culture medium (DMEM with 10% FBS). The results are shown in Fig.7. The release of the BMP-2 from the β-TCP/BMP-2 exhibited a rapid burst release followed by a slow accumulation profile. Approximately 20% of the initially loaded BMP-2 was released from the β-TCP/BMP-2 after the first 2 hrs, and around 50% after the first day, followed by a slow release during the subsequent 5 weeks (Fig.7). The release kinetics of the β-TCP/ECM-7/BMP-2 was similar to that of the β-TCP/BMP-2, though the cumulative percent of BMP-2 released was slightly lower than that of the β-TCP/BMP-2. However, in contrast, the burst release of the BMP-2 from the β-TCP/ECM-14/BMP-2 was significantly reduced. Approximately 10% of the BMP-2 was released from the β-TCP/ECM-14/BMP-2 after the first 2 hrs, and about 25% after the first day, and up to ~50% after the first 2 weeks, followed by a slower release in the following 3 additional weeks (Fig.7). Compared to the β-TCP and the β-TCP/ECM-7, the release of the BMP-2 from the β-TCP/ECM-14 demonstrated a significantly slower and more sustainable release profile over the entire time period of experiment.

3.4. Effect of released BMP-2 on F-actin distribution

The microfilamentous actins (F-actin) in hBMSC have been evaluated by immunofluorescent analysis after exposure to different microenvironments for 3 days. Fig. 8 shows F-actin morphology in the β-TCP and β-TCP/ECM groups with the presence and absence of BMP-2. The presence of BMP-2 released from the β-TCP and the β-TCP/ECM induced pronounced cytoskeletal reorganizations and F-actin augmentation (Fig. 8B, 8D, and 8F) compared to those without BMP-2 loading (Fig. 8A, 8C, and 8E). The effect of

BMP-2 on F-actin intensity of the cells was further assessed by immunofluorescent image analysis according to the intensity of fluorescent phalloidin signals. The results in Table 2 revealed that the mean values of the F-action signal of the cells in the presence of BMP-2 were significantly greater than those in the absence of BMP-2, regardless of substrates. The quantification of F-actin accumulation indicated that the BMP-2 released from scaffolds increased the accumulation of F-actin fibers.

3.5. Cell proliferation and differentiation

dsDNA content was used to indicate cell proliferation. Fig. 9 shows the proliferation of hBMSCs on the β-TCP, β-TCP/ECM-7, and β-TCP/ECM-14 in the absence (Fig.9A) and presence of BMP-2 (Fig.9B). It can be seen from Fig.9A that the dsDNA content on the β-TCP/ECM-7 was significantly greater than that on the β-TCP ($p< 0.05$), and the dsDNA content on the β-TCP/ECM-14 was significantly greater than that on the β-TCP ($p< 0.05$) and the β-TCP/ECM-7 ($p<0.05$) after 3 days of incubation. At day 7, the dsDNA contents on the β-TCP/ECM-7 and β-TCP/ECM-14 were significantly greater than that on the β-TCP ($p< 0.05$), and there was no significant difference between β-TCP/ECM-7 and the β-TCP/ECM-14 group. After 10 and 14 days of incubation, there was no significant difference among the 3 groups, suggesting the cells reached confluence on the scaffolds after 10 days of incubation. This implies that the ECM deposited on the β-TCP/ECM-7 and the β-TCP/ECM-14 significantly promoted the early proliferation of the hBMSC compared to the β-TCP. Fig.9B further indicates that the proliferation of hBMSC on the β-TCP/ECM-14/BMP-2 and the β-TCP/ECM-7/BMP-2 was significantly greater compared to the proliferation of those on the β-TCP/BMP-2 and the β-TCP/ECM-7 scaffolds at 3 days of incubation, which was consistent with the results in the absence of BMP-2 in Fig.9A. There is no significant difference in cell proliferation among the β-TCP/BMP-2, β-TCP/ECM-7/BMP-2, and β-TCP/ECM-14/BMP-2 after 7 days of incubation, suggesting the confluence of hBMSC grown on the scaffolds.

Alkaline phosphatase (ALP) is an early-stage marker of hBMSC differentiation to osteoblast cells. As shown in Fig.10, in the absence of BMP-2 the ECM alone did not promote the ALP production of hBMSCs during the period of experiment, whether the ECM was deposited on the scaffolds for 7 days or 14 days, compared to those on the β-TCP. However, at day 3, the hBMSCs on the β-TCP/BMP-2 and the β-TCP/ECM-7/BMP-2 expressed significantly higher ALP levels compared to the cells on the corresponding scaffolds without the presence of BMP-2. No significant difference in the ALP level was observed between the β-TCP/ECM-14 and the β-TCP/ECM-14/BMP-2. Furthermore, the ALP activity expression of the hBMSCs on the β-TCP/BMP-2 was significantly higher than that on the β-TCP/ECM-7/BMP-2, while the ALP level on the β-TCP/ECM-7/BMP-2 also was significantly higher than that on the β-TCP/ECM-14/BMP-2. At day 7, the three groups loaded with BMP-2 still promote significantly higher ALP production compared to those in the corresponding groups without loaded BMP-2, but differences among the three groups loaded with BMP-2 disappeared. At day 10, the ALP activity between the β-TCP and β-TCP/BMP-2 showed no significant difference, but the β-TCP/ECM-7/BMP-2 and the β-TCP/ECM-14/BMP-2 significantly promoted the ALP production compared to the β-TCP/BMP-2 and other three groups without BMP-2 loading. However, at day 14, only the β-TCP/ECM-14/BMP-2 exhibited significantly greater ALP activity expression than the β-TCP/BMP-2 and the β-TCP/ECM-14. Taken together, these results suggested that the β-TCP/BMP-2 had an initial burst release which resulted in a rapid and enhanced ALP expression at the early stage; however, the β-TCP/ECM-7/BMP-2 and the β-TCP/ECM-14/BMP-2 sustainably released the BMP-2, which significantly promoted the ALP expression long term.

3.6. Effects of β-TCP/ECM and β-TCP/ECM/BMP-2 on mineralization

We next investigated the ability of hBMSC to deposit calcium mineral nodules *in vitro* by Alizarin red S staining in the presence and absence of ECM and BMP-2 on CaP scaffold. Fig.11 shows the Alizarin Red S-stained calcium mineral nodules produced by hBMSCs after 14 and 21 days incubation in the presence of scaffolds with and without ECM and/or BMP-2 pre-loading. The results in Fig.11 demonstrate that the hBMSCs in the presence and absence of BMP-2 both deposited detectable calcium mineral nodules after 14 and 21 days of incubation (Fig.11). At day 14, the hBMSCs started to deposit small amounts of calcium mineral nodules, while more matrix deposition and calcium mineral nodules can be observed at day 21. At day 21, larger calcium mineral nodules were present in the BMP-2-loaded groups than those in the groups without BMP-2. Quantification of calcium mineral nodules is shown in Fig.12. At day 14, there was no difference in calcium ion concentration among all the groups. However, at day 21, the BMP-2-loaded groups demonstrated significantly greater calcium mineral content compared to the corresponding groups without BMP-2 loading (Fig.12). It is worth noting that the β-TCP/ECM-7/BMP-2 and β-TCP/ECM-14/BMP-2 exhibited significantly more mineral formation compared to that of the β-TCP/BMP-2 after 21 days of incubation.

4. Discussion

In bone tissue engineering, the ideal scaffold is one that has a 3D, interconnected porous network, provides a structural support for cell ingrowth and proliferation, and surface properties that provide microenvironmental and biological cues for cell functions. The template-casting method in this study enables the fabrication of an interconnected porous scaffold with controlled pore structure and porosities. The main objective of this study was to investigate whether the hBMSC-derived ECM on a biodegradable β-TCP scaffold can bind BMP-2 and control the release of BMP-2 in a sustained manner and, additionally, to examine the effect of ECM and the sustained released BMP-2 from the ECM on cell behaviors. First, we characterized the ECM deposited on the β-TCP scaffolds through SEM, XPS, FTIR and immunofluorescent staining. The SEM images show the changes of surface morphology of the scaffolds before and after cell culture (Fig.2). The immunofluoresecent staining images show the presence of collagen type I, a major component of ECM, on the β-TCP (Fig.3). The XPS and FTIR data demonstrate the appearance of hydroxyl groups, amino groups, and amide groups, three major functional groups of ECM, on the β-TCP (Figs. 4 and 5). Collectively, all the results indicate the presence of ECM on the β-TCP scaffolds. This simple process generates a biomimetic bony environment comprised of a cell-derived, natural ECM on a calcium mineral scaffold.

Next, we examined the loading and release kinetics of BMP-2 to and from the β-TCP, β-TCP/ECM-7, and β-TCP/ECM-14. Here we, for the first time, have demonstrated that the loading kinetics of the BMP-2 onto the β-TCP was significantly faster compared to the loading kinetics for the β-TCP/ECM-14 and the β-TCP/ECM-7 within the first 4 hours. The BMP-2 loading kinetics was also affected by the ECM content, as determined by the incubation time. In particular, within the first 30 minutes, the amounts of BMP-2 loaded on each scaffold were 73.64% on the β-TCP, 52.6% on the β-TCP/ECM-7, and 42.06% on the β-TCP/ECM-14. It is worth noting that after the initial 12 hours, there was no significant difference in the amount of BMP-2 loaded among the three groups, and all groups reached approximately 80% loading at that time point. On the other hand, the release of BMP-2 from the β-TCP was significantly faster compared to the β-TCP/ECM-14 and the β-TCP/ECM-7 within the first 7 days. In particular, the β-TCP/ECM-14 released the BMP-2 in a sustained manner without a burst release compared to the β-TCP (17.42% of BMP-2 released from the β-TCP/ECM-14 v.s. 31.02% from the β-TCP within the first 4 hours, $p<0.05$), while the β-TCP/ECM-7 demonstrated a slightly reduced initial release compared to the β-TCP (27.89%

from the β-TCP/ECM-7 vs. 31.02% from the β-TCP within the first 4 hours, $p>0.05$). The significant difference in the BMP-2 release profiles between the β-TCP/BMP-2 and the β-TCP/ECM-14/BMP-2 lasted for 1 week. These results clearly indicate a change in the interaction mechanisms between the BMP-2 and the β-TCP, β-TCP/ECM-7, or β-TCP/ECM-14. The *in vitro* release profiles suggest that the release kinetics of the BMP-2 could be controlled by the presence and content of the ECM. The interaction mechanism between the BMP-2 and the β-TCP was physical adsorption through microporous surfaces because the β-TCP lacks functional groups such as -OH [52]. Most of the BMP-2 was physically but weakly adsorbed on the surface, macropores, and micropores on the struts of the scaffolds. This probably explains the quick adsorption of the BMP-2 to the β-TCP and the initial burst release of the BMP-2 from the BMP-2-loaded β-TCP as shown in Fig.7. However, there are many functional groups in the ECM proteins, such as −OH, $-NH_2$, −COOH, and CON-, which potentially provide additional binding mechanisms or binding sites to growth factors, such as BMP-2, through strong Coulombic interactions and hydrogen bonding [52]. More importantly, the cell-derived natural ECM matrix is composed of a vast number of fibronectin, collagen and laminin molecules, which have heparin sulfate proteoglycan components. These components in the ECM have high affinity for heparin-binding growth factors, including BMP-2 [12]. Several studies have incorporated heparin binding growth factors such as BMP-2 into heparinized matrices [10, 11] by taking advantage of the higher affinity of the heparinized matrices compared to collagen alone. Studies also have shown that other similar growth factor family members, such as BMP-7 and TGF-β1, also bind with higher affinity to the basal lamina components collagen IV (highest affinity), laminin, and collagen I [53–55]. From those studies and our experiments, it is clear that the cell-derived natural ECM can provide multiple binding mechanisms, including heparin-specific binding with growth factors, and can potentially regulate the release of growth factors. With this in mind, we can say that the changes in the binding mechanisms between the BMP-2 and the β-TCP/ECM-7 or the β-TCP/ECM-14 are probably responsible for the slower loading and release kinetics of the BMP-2 compared to those of the β-TCP.

Optimized growth factor release kinetics can significantly improve therapeutic responses due to different dose requirements in different phases in physiological bone repair, i.e. the inflammatory, chondrogenic, and osteogenic phases [56]. The *in vitro* biological evaluation has indicated that the β-TCP/ECM-14/BMP-2 sustainably promoted the differentiation of the hBMSC by sustainably releasing the BMP-2, while the β-TCP/BMP-2 only had an initial boost of cell differentiation by an initial burst release of the BMP-2. Although more studies are needed to analyze the precise molecular interactions between the BMP-2 and the ECM with multiple components, the results suggest that the ECM could be used to control the release of the BMP-2 in a sustained manner and that the released BMP-2 was still biologically active and induced osteoblast differentiation. Due to the binding of growth factors to ECM components, the effects of growth factors and ECM are interdependent. When the cells were seeded on the ECM/ β-TCP, the cell surface-associated matrix metalloproteinase broke down the ECM, releasing the bound growth factors, which then carried out their biological roles. At the same time, the degradation of the β-TCP also partially released the ECM deposited on it, thus releasing the growth factors trapped in the ECM. Although it is still unclear whether the released amount of the BMP-2 was at the optimal dose for tissue regeneration, this *in vitro* release study has shown that the release of the BMP-2 could be regulated using the amount of the ECM deposited on the β-TCP at different culture times. These results further imply that natural ECM may function as a release carrier of multiple growth factors and this principle could be widely applied to create ECM with various maturities to control and enhance bioactivity.

Studies have indicated that a variety of matrix proteins such as osteopontin, thrombospondin, and bone sialoprotein are important in bone cell migration, proliferation,

matrix deposition, and mineralization [57]. As shown in Figs. 9 to 12, the β-TCP/ECM-7 and the β-TCP/ECM-14 significantly enhanced the cell proliferation at the initial time points, but not osteogenic differentiation and mineralization, as compared to the β-TCP. The enhancement of proliferation is probably due to the effect of matrix proteins. It is worth noting that the biodegradable β-TCP scaffolds may mask the enhanced calcium mineral deposition by cell-derived ECM compared to previous results on titanium and polymeric scaffolds [26–28]. In addition, the BMP-2 released from the ECM significantly enhanced the thickness and elongation of F-actin as shown in Fig.8 and Table 2. The accumulation of F-actin is an early and critical event in cell maturation and function [58]. This result was consistent with the previous report that BMP-2 induced reorganization of the actin cytoskeleton [46, 47]. As expected, the scaffolds with loaded BMP-2 promoted osteogenic differentiation and calcium mineral formation more than those without BMP-2 loading. More importantly, as shown in Figs. 10 and 12, the sustainable release of BMP-2 from the β-TCP/ECM-14/BMP-2 significantly enhanced osteogenic differentiation and mineral formation compared to the β-TCP/BMP-2. Therefore, bone matrix proteins deposited on the scaffold provided biological cues via cell-matrix interactions to promote cell growth and mineralization.

5. Conclusions

This work demonstrates a potential method for the creation of a bony microenvironment. The present results show that a cell-derived ECM on an interconnected porous biodegradable β-TCP scaffold significantly slows the loading and release kinetics of BMP-2 and regulates cell responses. Therefore, the cell-derived ECM on the β-TCP is a promising platform not only for providing biological cues for cell responses, but also for binding and controlling the release of single or multiple exogenous growth factors.

Acknowledgments

We would like to acknowledge the supports from March of Dimes Birth Defect Foundation, Airlift Research Foundation, Wallace H. Coulter Foundation, DOD W81XWH-10-1-0966, NIH R01AR057837 from NIAMS, and NIH R01DE021468 from NIDCR.

References

1. Wang L, Murthy SK, Barabino GA, Carrier RL. Synergic effects of crypt-like topography and ECM proteins on intestinal cell behavior in collagen based membranes. Biomaterials. 2010; 31:7586–98. [PubMed: 20643478]
2. Kleinman HK, Luckenbill-Edds L, Cannon FW, Sephel GC. Use of extracellular matrix components for cell culture. Anal Biochem. 1987; 166:1–13. [PubMed: 3314585]
3. Badylak SF, Freytes DO, Gilbert TW. Extracellular matrix as a biological scaffold material: Structure and function. Acta Biomater. 2009; 5:1–13. [PubMed: 18938117]
4. Anselme K. Osteoblast adhesion on biomaterials. Biomaterials. 2000; 21:667–81. [PubMed: 10711964]
5. Ivaska J, Heino J. Adhesion receptors and cell invasion: mechanisms of integrin-guided degradation of extracellular matrix. Cell Mol Life Sci. 2000; 57:16–24. [PubMed: 10949578]
6. Bi Y, Stuelten CH, Kilts T, Wadhwa S, Iozzo RV, Robey PG, et al. Extracellular matrix proteoglycans control the fate of bone marrow stromal cells. J Biol Chem. 2005; 280:30481–9. [PubMed: 15964849]
7. Pham QP, Kasper FK, Scott Baggett L, Raphael RM, Jansen JA, Mikos AG. The influence of an in vitro generated bone-like extracellular matrix on osteoblastic gene expression of marrow stromal cells. Biomaterials. 2008; 29:2729–39. [PubMed: 18367245]
8. Rozario T, DeSimone DW. The extracellular matrix in development and morphogenesis: a dynamic view. Dev Biol. 2010; 341:126–40. [PubMed: 19854168]

9. Reilly GC, Engler AJ. Intrinsic extracellular matrix properties regulate stem cell differentiation. J Biomech. 2010; 43:55–62. [PubMed: 19800626]
10. Wissink MJ, Beernink R, Pieper JS, Poot AA, Engbers GH, Beugeling T, et al. Binding and release of basic fibroblast growth factor from heparinized collagen matrices. Biomaterials. 2001; 22:2291–9. [PubMed: 11456069]
11. Pieper JS, Hafmans T, van Wachem PB, van Luyn MJ, Brouwer LA, Veerkamp JH, et al. Loading of collagen-heparan sulfate matrices with bFGF promotes angiogenesis and tissue generation in rats. J Biomed Mater Res. 2002; 62:185–94. [PubMed: 12209938]
12. Ruoslahti E, Yamaguchi Y. Proteoglycans as modulators of growth factor activities. Cell. 1991; 64:867–9. [PubMed: 2001586]
13. Wu YC, Shaw SY, Lin HR, Lee TM, Yang CY. Bone tissue engineering evaluation based on rat calvaria stromal cells cultured on modified PLGA scaffolds. Biomaterials. 2006; 27:896–904. [PubMed: 16125224]
14. Badylak S, Liang A, Record R, Tullius R, Hodde J. Endothelial cell adherence to small intestinal submucosa: an acellular bioscaffold. Biomaterials. 1999; 20:2257–63. [PubMed: 10614932]
15. Flynn LE, Prestwich GD, Semple JL, Woodhouse KA. Proliferation and differentiation of adipose-derived stem cells on naturally derived scaffolds. Biomaterials. 2008; 29:1862–71. [PubMed: 18242690]
16. Bhrany AD, Beckstead BL, Lang TC, Farwell DG, Giachelli CM, Ratner BD. Development of an esophagus acellular matrix tissue scaffold. Tissue Eng. 2006; 12:319–30. [PubMed: 16548690]
17. Narayanan K, Leck KJ, Gao S, Wan AC. Three-dimensional reconstituted extracellular matrix scaffolds for tissue engineering. Biomaterials. 2009; 30:4309–17. [PubMed: 19477508]
18. Li WJ, Tuli R, Huang X, Laquerriere P, Tuan RS. Multilineage differentiation of human mesenchymal stem cells in a three-dimensional nanofibrous scaffold. Biomaterials. 2005; 26:5158–66. [PubMed: 15792543]
19. Mauney JR, Kirker-Head C, Abrahamson L, Gronowicz G, Volloch V, Kaplan DL. Matrix-mediated retention of in vitro osteogenic differentiation potential and in vivo bone-forming capacity by human adult bone marrow-derived mesenchymal stem cells during ex vivo expansion. J Biomed Mater Res A. 2006; 79:464–75. [PubMed: 16752403]
20. Mistry AS, Mikos AG. Tissue engineering strategies for bone regeneration. Adv Biochem Eng Biotechnol. 2005; 94:1–22. [PubMed: 15915866]
21. Khademhosseini A, Vacanti JP, Langer R. Progress in tissue engineering. Sci Am. 2009; 300:64–71. [PubMed: 19438051]
22. Rosso F, Giordano A, Barbarisi M, Barbarisi A. From cell-ECM interactions to tissue engineering. J Cell Physiol. 2004; 199:174–80. [PubMed: 15039999]
23. Hubbell JA. Materials as morphogenetic guides in tissue engineering. Curr Opin Biotechnol. 2003; 14:551–8. [PubMed: 14580588]
24. Hersel U, Dahmen C, Kessler H. RGD modified polymers: biomaterials for stimulated cell adhesion and beyond. Biomaterials. 2003; 24:4385–415. [PubMed: 12922151]
25. Beck K, Hunter I, Engel J. Structure and function of laminin: anatomy of a multidomain glycoprotein. FASEB J. 1990; 4:148–60. [PubMed: 2404817]
26. Datta N, Holtorf HL, Sikavitsas VI, Jansen JA, Mikos AG. Effect of bone extracellular matrix synthesized in vitro on the osteoblastic differentiation of marrow stromal cells. Biomaterials. 2005; 26:971–7. [PubMed: 15369685]
27. Datta N, Pham QP, Sharma U, Sikavitsas VI, Jansen JA, Mikos AG. In vitro generated extracellular matrix and fluid shear stress synergistically enhance 3D osteoblastic differentiation. Proc Natl Acad Sci U S A. 2006; 103:2488–93. [PubMed: 16477044]
28. Thibault RA, Scott Baggett L, Mikos AG, Kasper FK. Osteogenic differentiation of mesenchymal stem cells on pregenerated extracellular matrix scaffolds in the absence of osteogenic cell culture supplements. Tissue Eng Part A. 2010; 16:431–40. [PubMed: 19863274]
29. Einhorn TA. The cell and molecular biology of fracture healing. Clin Orthop Relat Res. 1998:S7–21. [PubMed: 9917622]
30. Babensee JE, McIntire LV, Mikos AG. Growth factor delivery for tissue engineering. Pharm Res. 2000; 17:497–504. [PubMed: 10888299]

31. Woo BH, Fink BF, Page R, Schrier JA, Jo YW, Jiang G, et al. Enhancement of bone growth by sustained delivery of recombinant human bone morphogenetic protein-2 in a polymeric matrix. Pharm Res. 2001; 18:1747–53. [PubMed: 11785696]
32. Fromigue O, Marie PJ, Lomri A. Bone morphogenetic protein-2 and transforming growth factor-beta2 interact to modulate human bone marrow stromal cell proliferation and differentiation. J Cell Biochem. 1998; 68:411–26. [PubMed: 9493905]
33. Lecanda F, Avioli LV, Cheng SL. Regulation of bone matrix protein expression and induction of differentiation of human osteoblasts and human bone marrow stromal cells by bone morphogenetic protein-2. J Cell Biochem. 1997; 67:386–96. [PubMed: 9361193]
34. Groeneveld EH, Burger EH. Bone morphogenetic proteins in human bone regeneration. Eur J Endocrinol. 2000; 142:9–21. [PubMed: 10633215]
35. Hollinger JO, Schmitt JM, Buck DC, Shannon R, Joh SP, Zegzula HD, et al. Recombinant human bone morphogenetic protein-2 and collagen for bone regeneration. J Biomed Mater Res. 1998; 43:356–64. [PubMed: 9855194]
36. Bishop GB, Einhorn TA. Current and future clinical applications of bone morphogenetic proteins in orthopaedic trauma surgery. Int Orthop. 2007; 31:721–7. [PubMed: 17668207]
37. Cancedda R, Giannoni P, Mastrogiacomo M. A tissue engineering approach to bone repair in large animal models and in clinical practice. Biomaterials. 2007; 28:4240–50. [PubMed: 17644173]
38. Luginbuehl V, Meinel L, Merkle HP, Gander B. Localized delivery of growth factors for bone repair. Eur J Pharm Biopharm. 2004; 58:197–208. [PubMed: 15296949]
39. Kirker-Head CA. Potential applications and delivery strategies for bone morphogenetic proteins. Adv Drug Deliv Rev. 2000; 43:65–92. [PubMed: 10967222]
40. Grellier M, Bordenave L, Amedee J. Cell-to-cell communication between osteogenic and endothelial lineages: implications for tissue engineering. Trends Biotechnol. 2009; 27:562–71. [PubMed: 19683818]
41. Li J, Zhang YP, Kirsner RS. Angiogenesis in wound repair: angiogenic growth factors and the extracellular matrix. Microsc Res Tech. 2003; 60:107–14. [PubMed: 12500267]
42. Amoroso A, Del Porto F, Di Monaco C, Manfredini P, Afeltra A. Vascular endothelial growth factor: a key mediator of neoangiogenesis. A review. Eur Rev Med Pharmacol Sci. 1997; 1:17–25. [PubMed: 9444794]
43. Liu Y, Kim JH, Young D, Kim S, Nishimoto SK, Yang Y. Novel template-casting technique for fabricating beta-tricalcium phosphate scaffolds with high interconnectivity and mechanical strength and in vitro cell responses. J Biomed Mater Res A. 2010; 92:997–1006. [PubMed: 19296544]
44. Zhao J, Zhang N, Prestwich GD, Wen X. Recruitment of endogenous stem cells for tissue repair. Macromol Biosci. 2008; 8:836–42. [PubMed: 18528846]
45. Jiang T, Abdel-Fattah WI, Laurencin CT. In vitro evaluation of chitosan/poly(lactic acid-glycolic acid) sintered microsphere scaffolds for bone tissue engineering. Biomaterials. 2006; 27:4894–903. [PubMed: 16762408]
46. Shah AK, Lazatin J, Sinha RK, Lennox T, Hickok NJ, Tuan RS. Mechanism of BMP-2 stimulated adhesion of osteoblastic cells to titanium alloy. Biol Cell. 1999; 91:131–42. [PubMed: 10399828]
47. Gamell C, Osses N, Bartrons R, Ruckle T, Camps M, Rosa JL, et al. BMP2 induction of actin cytoskeleton reorganization and cell migration requires PI3-kinase and Cdc42 activity. J Cell Sci. 2008; 121:3960–70. [PubMed: 19001503]
48. Stanford CM, Jacobson PA, Eanes ED, Lembke LA, Midura RJ. Rapidly forming apatitic mineral in an osteoblastic cell line (UMR 106-01 BSP). J Biol Chem. 1995; 270:9420–8. [PubMed: 7721867]
49. Wen F, Chang S, Toh YC, Teoh SH, Yu H. Development of poly (lactic-co-glycolic acid)-collagen scaffolds for tissue engineering. Mater Sci Eng C Mater Biol Appl. 2007; 27:285–92.
50. Yang MC, Wang SS, Chou NK, Chi NH, Huang YY, Chang YL, et al. The cardiomyogenic differentiation of rat mesenchymal stem cells on silk fibroin-polysaccharide cardiac patches in vitro. Biomaterials. 2009; 30:3757–65. [PubMed: 19410289]

51. Coelho PG, Coimbra ME, Ribeiro C, Fancio E, Higa O, Suzuki M, et al. Physico/chemical characterization and preliminary human histology assessment of a β-TCP particulate material for bone augmentation. Mater Sci Eng C Mater Biol Appl. 2009; 29:2085–91.

52. Dong X, Wang Q, Wu T, Pan H. Understanding adsorption-desorption dynamics of BMP-2 on hydroxyapatite (001) surface. Biophys J. 2007; 93:750–9. [PubMed: 17617550]

53. Vukicevic S, Latin V, Chen P, Batorsky R, Reddi AH, Sampath TK. Localization of osteogenic protein-1 (bone morphogenetic protein-7) during human embryonic development: high affinity binding to basement membranes. Biochem Biophys Res Commun. 1994; 198:693–700. [PubMed: 8297380]

54. Paralkar VM, Vukicevic S, Reddi AH. Transforming growth factor beta type 1 binds to collagen IV of basement membrane matrix: implications for development. Dev Biol. 1991; 143:303–8. [PubMed: 1991553]

55. Zhang H, Tasnim F, Ying JY, Zink D. The impact of extracellular matrix coatings on the performance of human renal cells applied in bioartificial kidneys. Biomaterials. 2009; 30:2899–911. [PubMed: 19217158]

56. Cho TJ, Gerstenfeld LC, Einhorn TA. Differential temporal expression of members of the transforming growth factor beta superfamily during murine fracture healing. J Bone Miner Res. 2002; 17:513–20. [PubMed: 11874242]

57. Shin H, Jo S, Mikos AG. Biomimetic materials for tissue engineering. Biomaterials. 2003; 24:4353–64. [PubMed: 12922148]

58. Hu T, Ramachandrarao SP, Siva S, Valancius C, Zhu Y, Mahadev K, et al. Reactive oxygen species production via NADPH oxidase mediates TGF-beta-induced cytoskeletal alterations in endothelial cells. Am J Physiol Renal Physiol. 2005; 289:F816–25. [PubMed: 16159901]

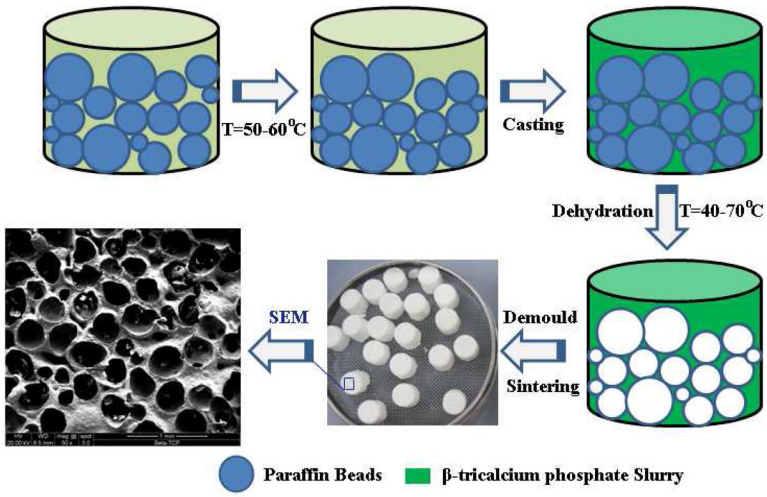

Fig.1.
The schematic graph of fabricating the β-TCP scaffolds and the SEM image of the β-TCP scaffold.

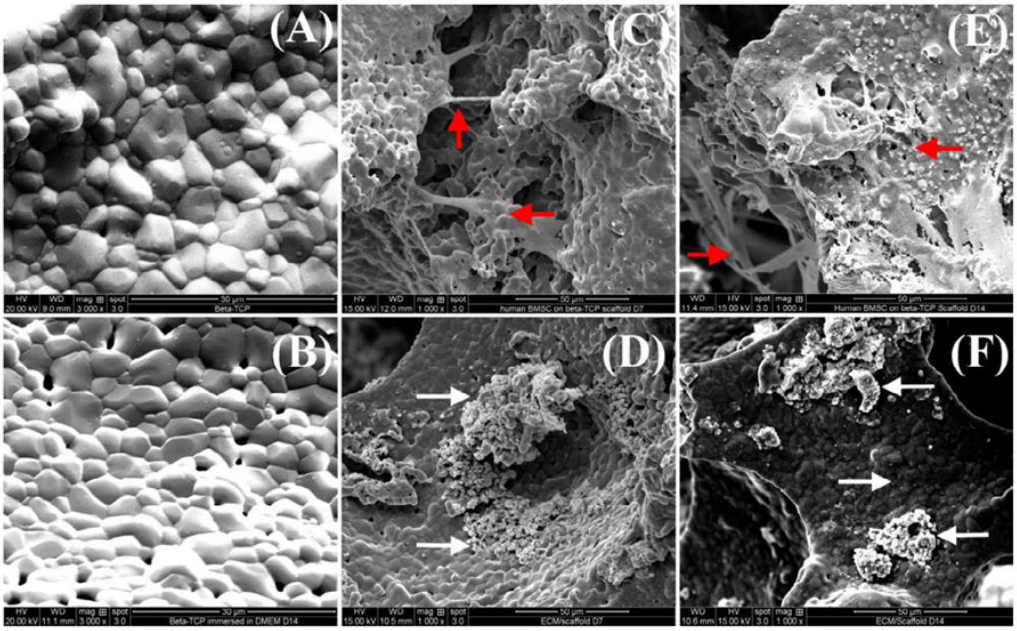

Fig.2.

SEM morphological observation of the β-TCP scaffolds, hBMSCs cultured on the scaffolds, and ECM produced by hBMSCs on the scaffolds. (A) β-TCP scaffolds; (B) β-TCP scaffolds after 14 days of immersion in cell culture medium; (C) cells on the scaffolds after 7 days of incubation; (D) decellularized scaffolds after 7 days of incubation; (E) cells on the scaffolds after 14 days of incubation; (F) decellularized scaffolds after 14 days of incubation. Note: The red arrows indicate the representative hBMSCs grown on the β-TCP scaffolds, and the white arrows indicate ECM produced by hBMSCs on the scaffold in either aggregates or layers

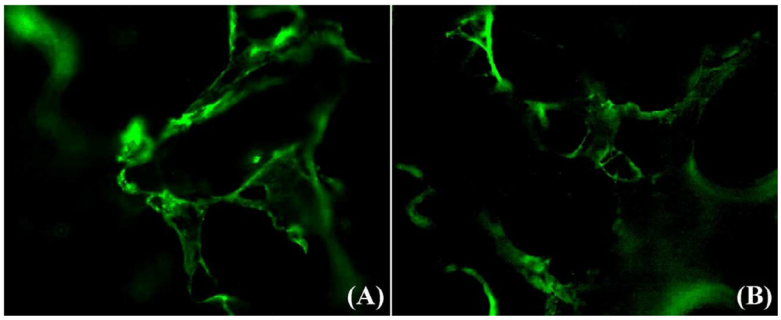

Fig.3.
Representative immunefluorescent images of collagen type I on the β-TCP scaffolds (A) after decellularization and (B) after EO gas sterilization.

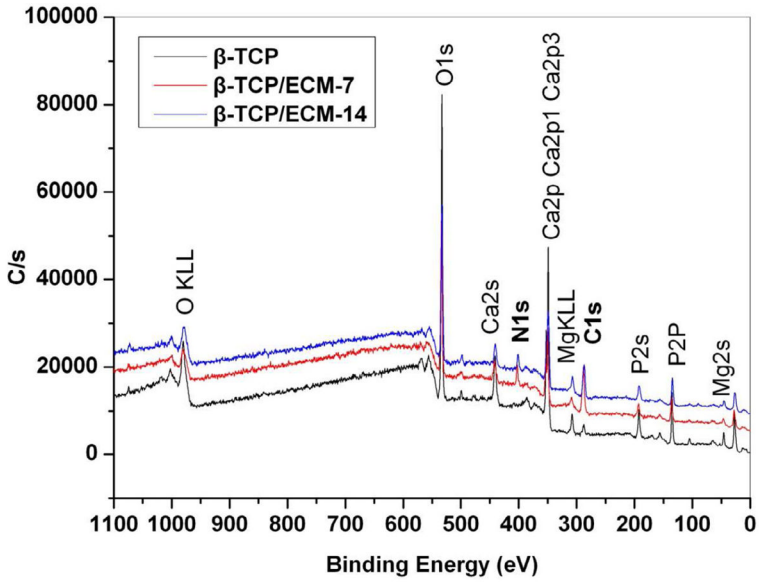

Fig. 4.
XPS spectra for the β-TCP, β-TCP/ECM-7, and β-TCP/ECM-14.

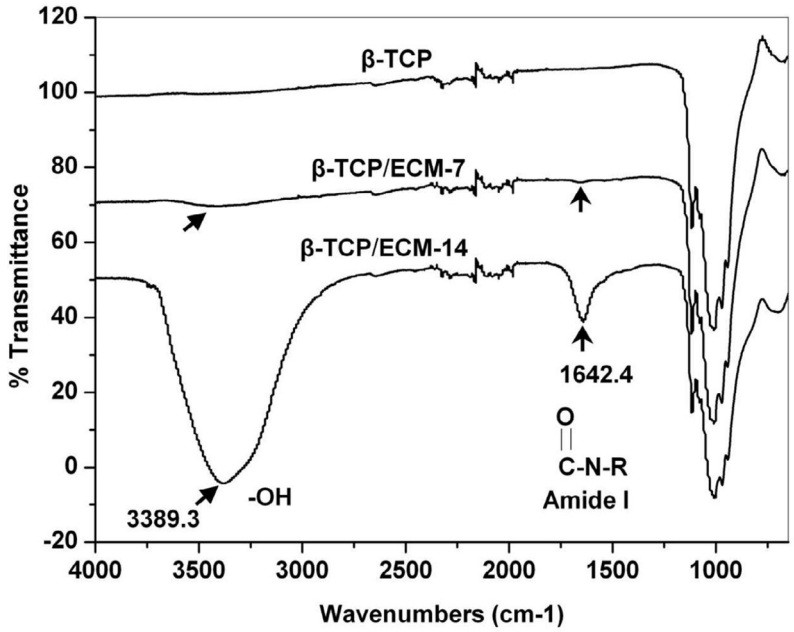

Fig. 5.

ATR-FTIR transmission spectra of the β-TCP, β-TCP/ECM-7, and β-TCP/ECM-14. The characteristic peaks of amide and hydroxyl groups are shown on the β-TCP/ECM-7 and the β-TCP/ECM-14 spectrum, respectively.

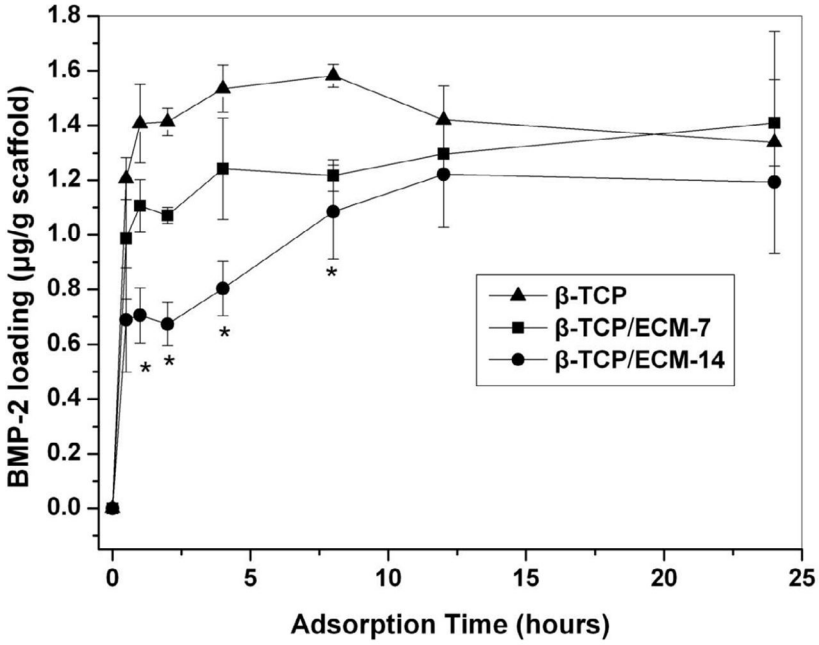

Fig. 6.
Loading kinetics of the BMP-2 onto the β-TCP, β-TCP/ECM-7, and β-TCP/ECM-14 in DMEM medium.

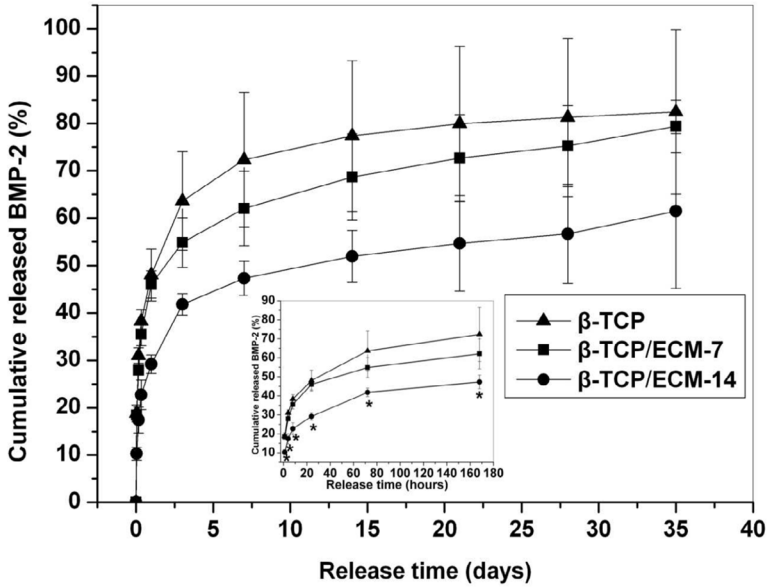

Fig. 7.

Cumulative release of BMP-2 from the β-TCP, β-TCP/ECM-7, and β-TCP/ECM-14 in DMEM medium. The data are presented as mean ± deviation (n=3). Significant difference is labeled as* in the insert (p<0.05).

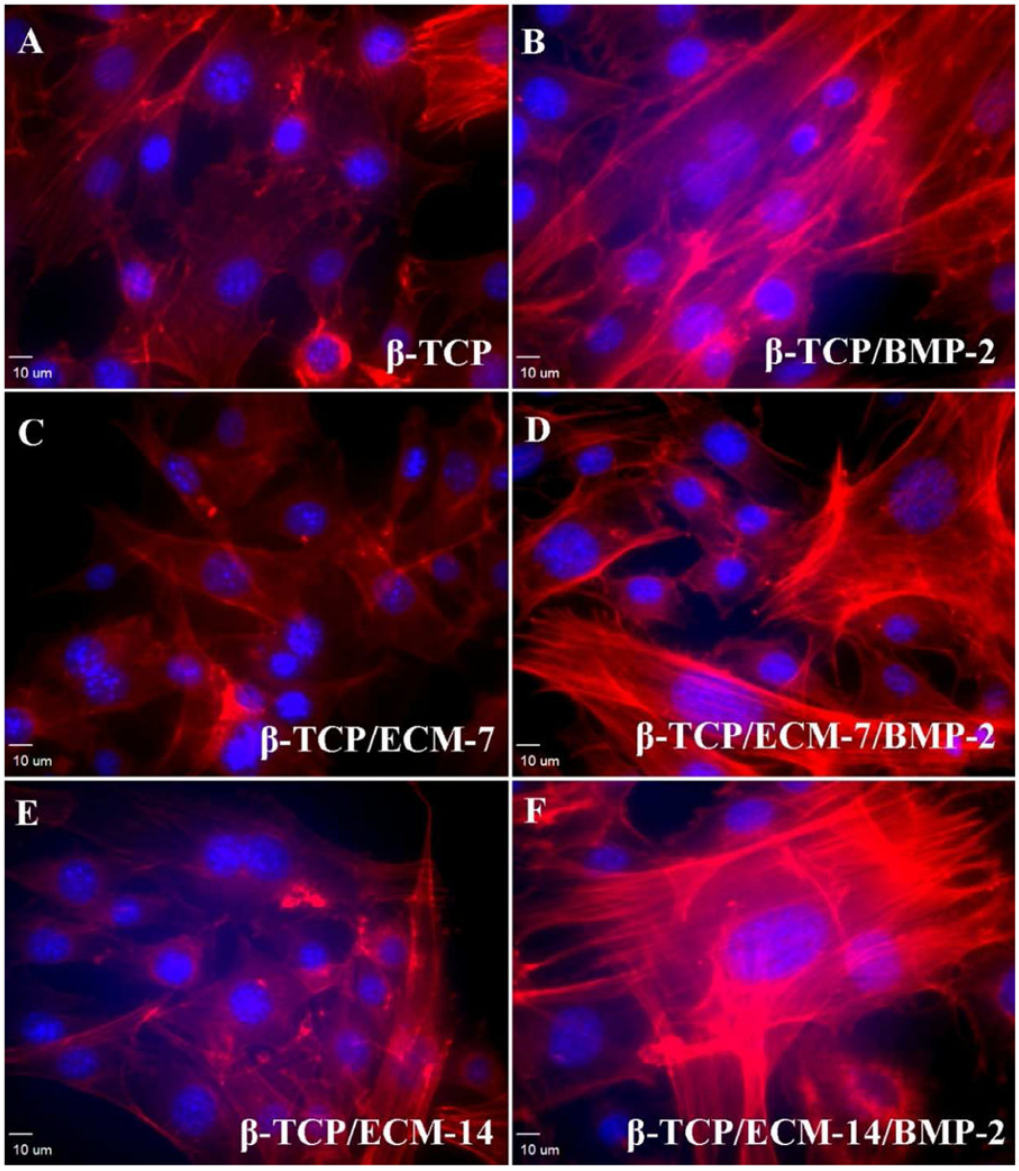

Fig. 8.

Representative immunofluorescent images for F-actin distribution in hBMSCs taken by a confocal laser scanning microscope after 3 days incubation. (A) Cells in the β-TCP scaffolds group; (B) Cells in the BMP-2-loaded β-TCP scaffolds; (C) Cells in the β-TCP/ECM-7 scaffolds; (D) Cells in the BMP-2-loaded β-TCP/ECM-7 scaffolds; (E) Cells in the β-TCP/ECM-14 scaffolds; and (F) Cells in the BMP-2-loaded β-TCP/ECM-7 scaffolds. Magnification: 20×; scale bar: 10 μm.

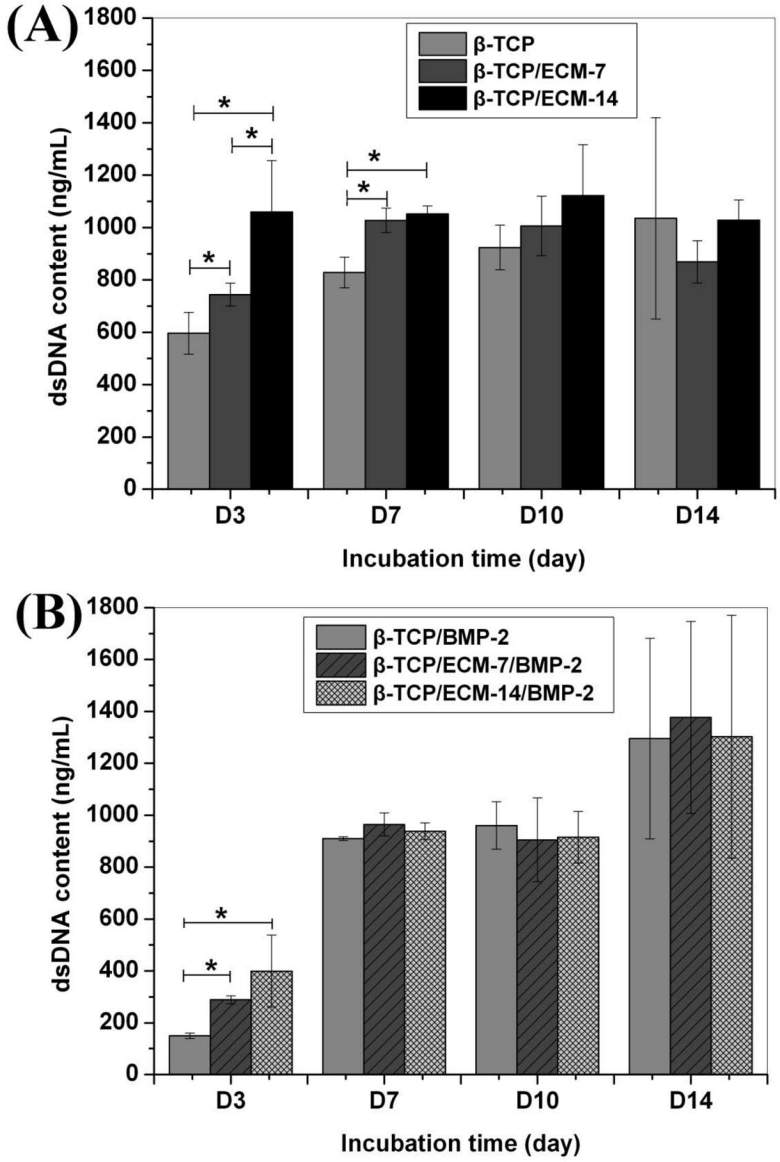

Fig.9.

The amount of dsDNA content synthesized by hBMSC grown over time on the β-TCP, β-TCP/ECM-7, and β-TCP/ECM-14 (A) in the absence of BMP-2 and (B) in the presence of BMP-2. Data are presented as mean ± standard deviation (n = 3). A * is marked to show the significant difference between groups ($p < 0.05$).

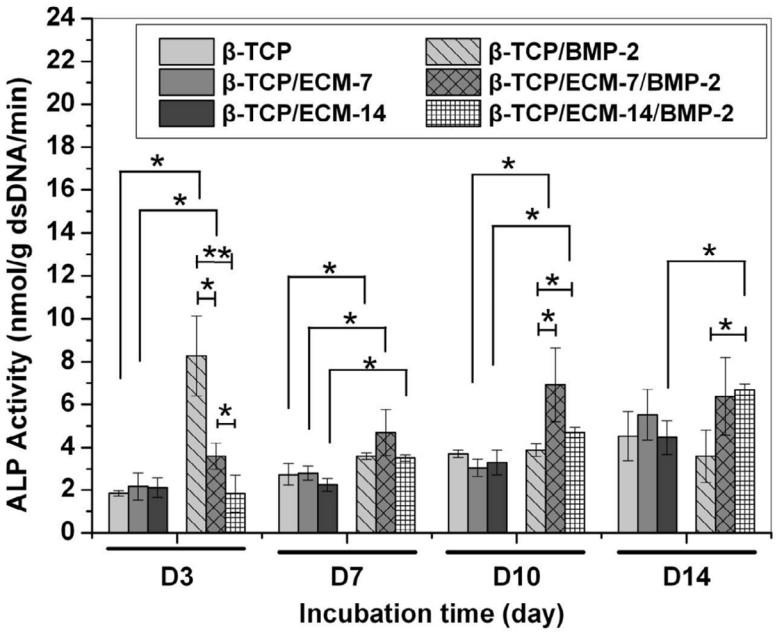

Fig.10.

Alkaline phosphatase activity of the hBMSCs on the β-TCP, β-TCP/ECM-7, and β-TCP/ECM-14 in the absence and presence of BMP-2. Data are presented as mean ± standard deviation (n = 3). A * is marked to show the significant difference between groups ($p < 0.05$).

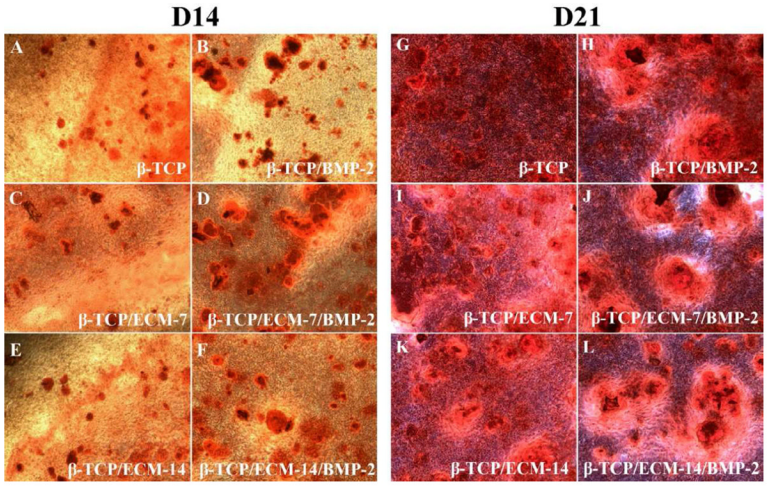

Fig.11.

Alizarin Red S-stained calcium mineral nodules deposited by the hBMSCs after incubation for 14 and 21 days in the absence and presence of ECM and/or BMP-2. (A, G) β-TCP scaffolds without BMP-2; (B, H) β-TCP scaffolds with BMP-2; (C, I) β-TCP/ECM-7 scaffolds without BMP-2; (D, J) β-TCP/ECM-7 scaffolds with BMP-2; (E, K) β-TCP/ECM-14 scaffolds without BMP-2; (F, L) β-TCP/ECM-14 scaffolds with BMP-2.

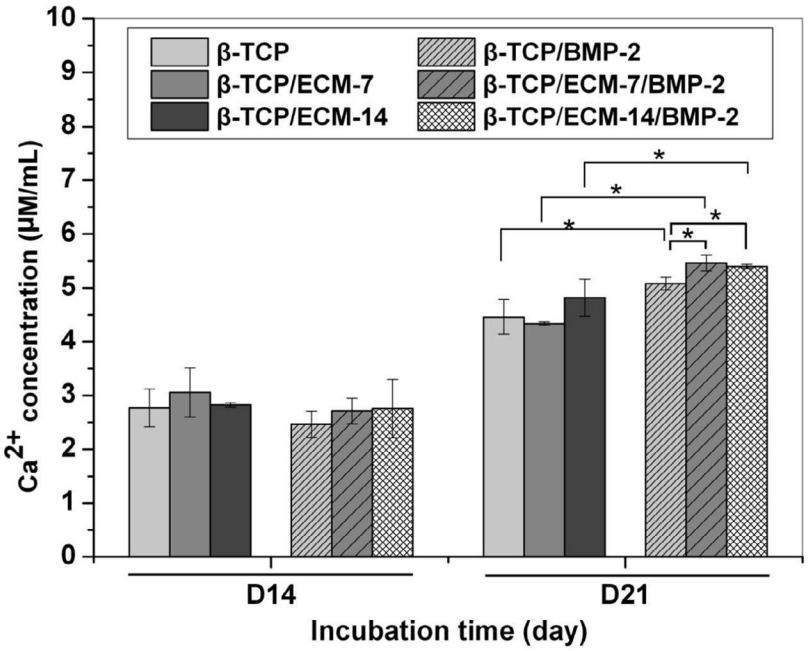

Fig.12.

Calcium content extracted from the mineralized matrix produced by hBMSCs after incubation for 14 and 21 days in the absence and presence of ECM and/or BMP-2. Data are presented as mean ± standard deviation. A * is marked to show the significant difference between groups ($p < 0.05$).

Table 1

The atomic percent of individual elements on the surface of the scaffolds automatically calculated by the software Multipak associated with the equipment.

Groups	Ca2p	P2p	O1s	C1s	N1s	Si2p	Mg2s
β-TCP	16.2	13	61	6.5	0	3.3	<0.1
β-TCP/ECM-7	8.1	6.8	39	39.1	6.4	0.5	<0.1
β-TCP/ECM-14	10.4	9.4	45.1	26.9	8.2	<0.1	<0.1

Table 2

The mean value of the intensity of F-actin signal in cells treated with Rhodamine phalloidin staining. Fluorescence intensity analysis was based on at least six random fields/well (three specimens for each experimental group) and the densities in TRITC and DAPI value were measured. Data are presented as mean ± standard error. Fluorescence of the sample with BMP-2 loading was significantly higher than that in the sample without BMP-2 loading ($p<0.05$).

Groups	F-actin Fluorescent Intensity(ADU/per cell)	
	Without BMP-2 loading	With BMP-2 loading
β-TCP	80.70 ± 6.11	121.01 ± 12.90*
β-TCP/ECM-7	92.16 ± 25.42	142.61 ± 25.48*
β-TCP/ECM-14	76.82 ± 9.84	131.45 ± 34.87*

A * is marked to show the significant difference between groups ($p < 0.05$).